A Plausible Model of Phyllotaxis - Supporting Text

Supporting Materials and Methods

Lines. All *Arabidopsis thaliana* lines were in the Columbia background. The *pin1* mutant allele used was *pin1-7*. *DR5::GFP* refers to the *DR5rev::GFP* line (1), in which the *DR5* promoter consists of nine repeats of the DR5 element (2), fused in inverse orientation to the minimal CaMV 35S promoter and the coding sequence of an endoplasmic-reticulum-targeted eGFP protein. This construct was kindly provided by J. Friml (Universität Tübingen, Tübingen, Germany) and crossed into the *pin1-7* background.

Treatments. *N*-1-naphthylphthalamic acid (NPA, 100 mM) and sirtinol (10 mM) stock solutions in dimethylsulphoxide (DMSO) were dissolved in half-strength MS medium (Serva, catalog no. 47515) to a final concentration of 20 μM and 25 μM, respectively. As a control, plates containing the same volume of DMSO dissolved in the medium were used. Immediately after dissection, the inflorescence meristems were grown on these plates or on normal one-half MS plates for 4, 24, or 48 h and then observed for *DR5::GFP* expression.

Confocal Microscopy. *DR5::GFP* expression patterns were studied by using a Leica upright confocal laser-scanning microscope (DMRXE7), equipped with a long-working-distance water immersion objective (×L63/0.90 U-V-I). The selected wavelengths were 500–550 nm for GFP and 620–690 nm for chlorophyll (used to check the specificity of the GFP signal).

Divergence Angle Measurements. Divergence angles were measured from sequential photographs taken at 2-day intervals beginning with seedlings 10 days after germination. A minimum of 22 plants was measured for each angle.

Computer Programming. Simulation models were implemented by using the VV programming environment (3), which extends the C++ language with support for specifying and visualizing dynamically changing cellular structures. Movies were assembled from sequences of frames output by VV with the TMPGENC video editing software. All simulations were performed on a 3 GHz Pentium 4 PC with an ATI Radeon 9000 graphics card.

Geometric Model of a Growing Meristem

Leaf initiation takes place in the peripheral zone of a growing shoot apical meristem and involves the patterning of cells that are rapidly dividing. According to the molecular data, the L1 layer plays a key role in this process. For the purposes of simulation, we treat this layer as a curved surface of negligible thickness, which allows us to simplify the problem of morphogenesis from three dimensions to two (4). The geometric model has four components: a model of the basic shape of the apex, a model of apex growth, a model of primordium outgrowth, and a model of cell shape and division.

The shape of the shoot apex is approximated as a rotationally symmetric reference surface (5–7) with superimposed outward-growing primordia (Fig. 7*A*). The reference surface is an idealization of the shape of the apex in the absence of primordia.

Growth of the reference surface is simulated by moving points embedded in it basipetally while maintaining the overall surface shape. This process is characterized by a relative elementary rate of growth function RERG(x), which defines the rate of elongation of infinitesimal segments of the generating curve as a function of their distance from the apex tip (6, 8, 9). The velocity with which surface points move away from the tip is obtained by integrating the RERG function along the generating curve. Following experimental data (10, 11), the RERG distribution is chosen such that the growth in the central zone is slower than in the peripheral zone.

Primordia are modeled as growing, rotationally symmetric bulges on the reference surface (Fig. 7*A*). A primordium center is placed at the average of the centroids of two adjacent cells that have an IAA concentration above the primordium differentiation threshold, *Th*. The radius *r* and height *h* of the primordium increase with the primordium age. These parameters act as scaling factors for a sigmoidal curve that defines the longitudinal cross section of the primordium.

Cells are modeled as polygons, following the method of Nakielski (5). The position of cell vertices changes over time as a result of the growth of the reference surface and gradual protrusion of primordia (Fig. 7*A*). Cell division occurs when the parent cell size (polygon area) reaches a threshold value. By default, the dividing wall is the shortest wall that passes through the centroid of the cell polygon. This position may be adjusted to avoid four-way junctions, which are unusual (11). To produce more realistic cell shapes, the vertices of the dividing wall are slightly moved toward each other (Fig. 7*B*). As observed by Nakielski (5), the dynamics of cell division and the resulting cellular patterns are similar to those observed in the *Arabidopsis* meristem (10, 11). We thus consider them an adequate structural support for modeling the auxin fluxes and PIN1 localization during phyllotactic pattern formation.

Sensitivity Analysis

To provide insight into the form and role of parameters in the model equations, we performed a preliminary sensitivity analysis. Starting with the parameter values for the spiral phyllotaxis simulation (column *Spiral* in Table 1), selected equations or parameters of the model were changed, and simulations were run again to determine whether spiral phyllotaxis could be maintained. Invariably, additional parameters needed to be adjusted, but an attempt was made to minimize their number. We focused on the analysis of pattern maintenance rather than pattern initiation. Consequently, the simulations were started by placing 10 initial primordia in a spiral pattern. Four simulated experiments were considered, and the divergence angles of primordia 11–20 observed (Table 3).

Fixed PIN1 Concentration. In this simulation, the equation for PIN1 production and decay (Eq. **1**) was removed from the model, and PIN1 concentration was fixed at 0.94,

the approximate value for nonprimordium cells in the original spiral model. Spiral phyllotaxis was maintained after decreasing IAA proximal zone production $\rho_{IAA}(proximal)$ from 3.0 to 2.5 and additional IAA production within primordia $\rho_{IAA}(primordium)$ from 3.5 to 2.5. The resulting sequence of divergence angles is listed in row SA1 of Table 3.

After fixing PIN1 concentration, the new parameter values that resulted in pattern maintenance were not difficult to find. On this basis, we concluded that the exact form of Eq. **1** is not critical to phyllotactic pattern formation.

Removal of IAA Production Saturation Term. According to Eqs. **5** and **6**, high IAA concentration saturates IAA production. We investigated the case when no saturation was present by setting the IAA production saturation coefficient κ_{IAA} to zero. Spiral phyllotaxis was maintained after reducing IAA proximal zone production $\rho_{IAA}(proximal)$ from 3.0 to 1.0, IAA production in the peripheral zone $\rho_{IAA}(peripheral)$ from 3.0 to 0.9, and additional IAA production within primordia $\rho_{IAA}(primordium)$ from 3.5 to 1.0 (simulation SA2 in Table 3).

As in the case of the simulation assuming fixed PIN1 concentration, it was not difficult to find parameter values that lead to the maintenance of spiral phyllotaxis. However, with κ_{IAA} set to zero, the model was no longer able to reproduce the *pin1* mutant phenotype. The IAA concentration was building up, leading to continuous formation of primordia that were completely filling the peripheral zone.

Reduction of Transport Exponent. The numerator in the IAA transport equation (Eq. **3**) specifies that the flux of IAA out of a source cell *i* is proportional to the square of the IAA concentration in this cell. Similarly, the denominator specifies that the flux of IAA to a destination cell *j* depends on the square of the IAA concentration in that cell.

To investigate whether the model critically depends on these quadratic relations, we decreased the exponent value from 2.0 to 1.5. The spiral phyllotaxis was maintained after reducing the transport coefficient T' from 22.5 to 19.0, the primordium differentiation threshold *Th* from 7.5 to 7.0, and the peripheral zone size from 2.9 to 2.57 (simulation SA3 in Table 3) . However, the model was very sensitive to parameter values, possibly due to the reduced cell count in the smaller peripheral zone.

Increase in PIN1 Relocation Exponent. The PIN1 polarization equation (Eq. **2**) gives an exponential preference to the neighbor cells with the highest IAA concentration. Experiments with other formulas, in which the polarization depended on the neighbor IAA concentration according to a linear or power function, did not yield spiral phyllotactic patterns.

To investigate how critically the model depends on the value of the exponentiation base *b* (Eq. **2**), we increased it from 3.0 to 4.0. Spiral phyllotaxis was maintained after increasing diffusion coefficient *D* from 4.0 to 4.5 and decreasing transport coefficient *T* from 22.5 to 22 (simulation SA4 in Table 3), but the simulation was very sensitive to

parameter values. Further experiments have shown that decussate and tricussate patterns could be obtained for *b* values as high as 5.0, but spiral simulations were most stable at values close to 3.0. Reducing the exponentiation base *b* below 2.5 did not yield spiral phyllotactic patterns.

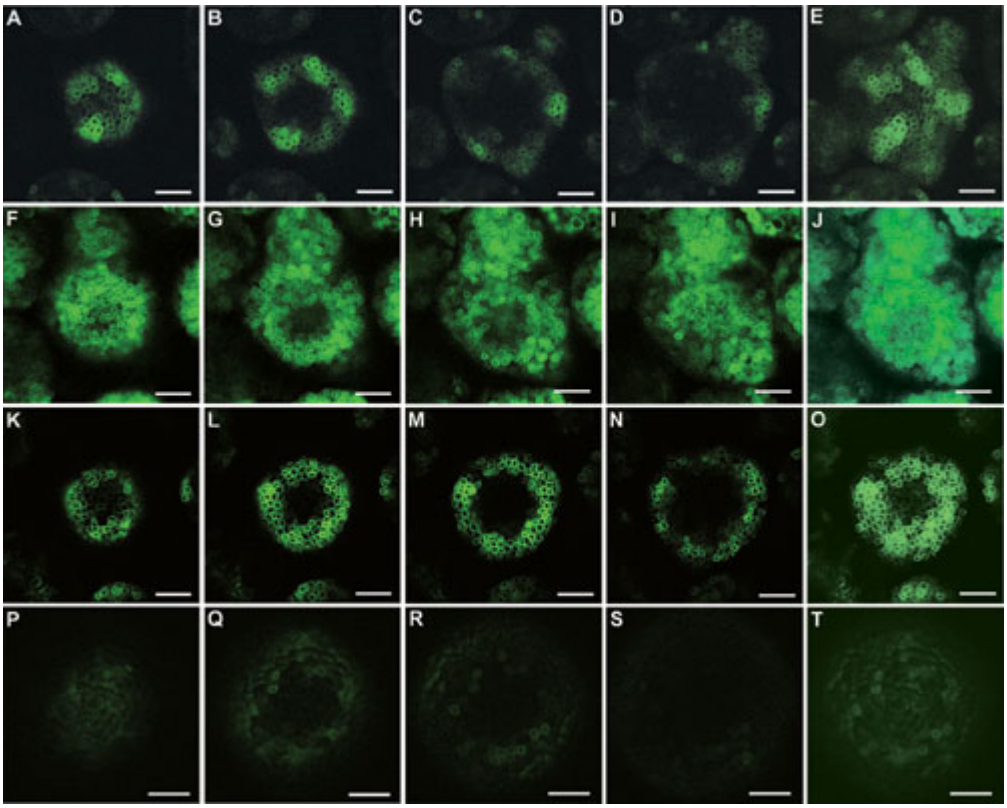

Fig. 6. Series of transverse optical sections through *DR5::GFP*-expressing inflorescence meristems, followed by the overlay of these sections (*E*, *J*, *O*, and *T*). (*A–E*) Wild-type inflorescence meristem. (*F–J*) Wild-type inflorescence meristem treated with 25 μM sirtinol during 48 h. (*K–O*) Wild-type inflorescence meristem treated with 20 μM naphthylphthalamic acid (NPA) during 24 h. (*P–T*) Inflorescence meristem of a *pin1-7* mutant. (Scale bars: 25 μm.)

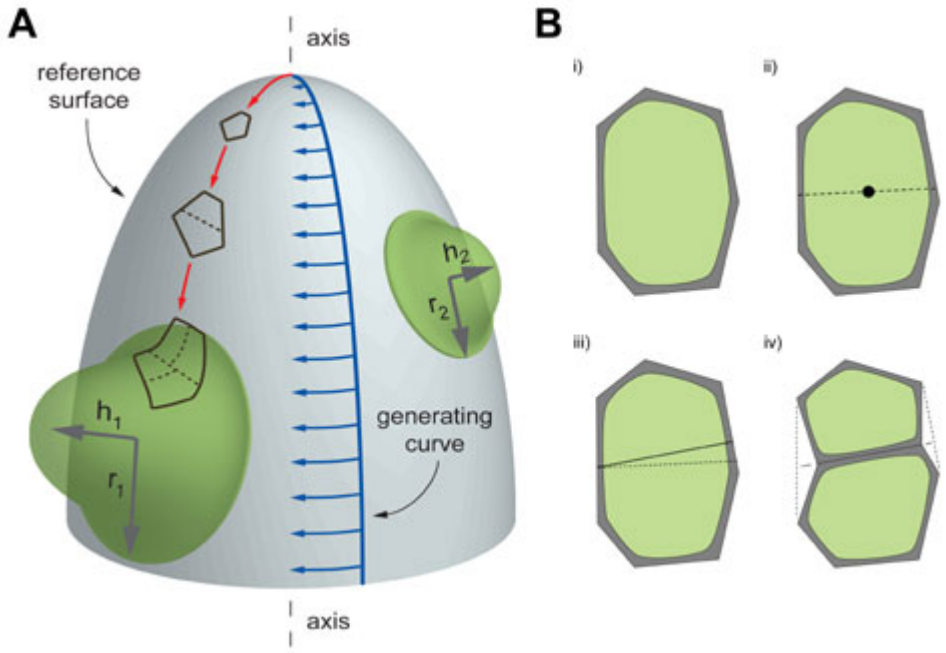

Fig. 7. (*A*) Geometric model of the shoot apical meristem. The reference surface is obtained by revolving a generating curve around the surface axis. Primordia (green) are modeled as smaller surfaces of revolution, protruding from the reference surface. Growth of the reference surface is modeled as a flow and elongation of surface elements (red arrows). This flow also defines the gradual displacement of the primordia over time, as their radius r and height h gradually increase ($r_1 > r_2$ and $h_1 > h_2$). Cells (dark polygons) grow as a result of the expansion of the apex surface and divide upon reaching the maximum size. (*B*) Details of the model of cell division. (*i*) The mother cell before division. (*ii*) The tentative dividing wall is the shortest wall passing through the centroid of the mother cell. (*iii*) The endpoints of the tentative wall are displaced from the vertices of the mother cell. (*iv*) The form of daughter cells is adjusted by shortening the dividing wall.

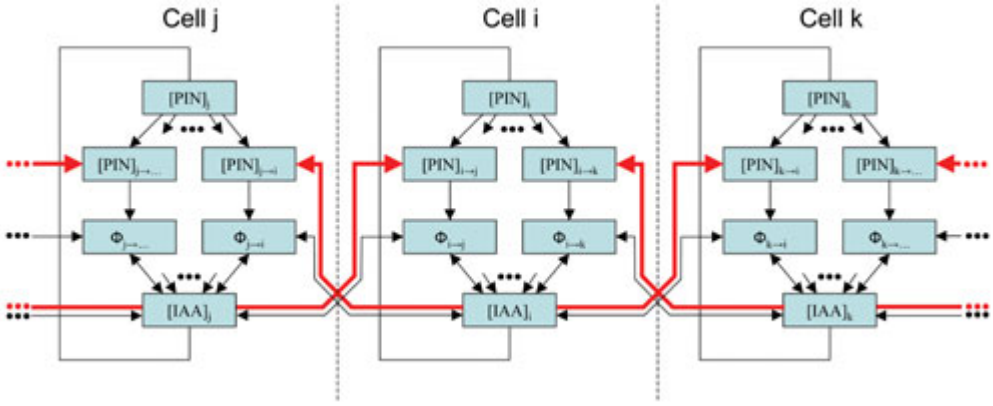

Fig. 8. Hypothetical feedback loops in cell polarization and auxin transport. A sample cell i and two of its neighbors, cells j and k, are shown. PIN1 molecules in each cell are distributed between cell membranes according to auxin concentration in the neighboring

cells (control information shown in red). The resulting auxin fluxes Φ modify auxin concentrations in each cell. These concentrations affect, in turn, both the concentration of PIN1 molecules in a given cell and distribution of PIN1 molecules in the neighboring cells. The model includes two types of feedback loops: local to a cell and spatially distributed, involving neighboring cells.

Table 1. Model parameters for phyllotaxis simulations

Parameter		Eq.	Distichous	Decussate	Tricussate	Spiral
IAA production coefficient in the proximal zone	$\rho_{IAA}(proximal)$	5	1.000	1.000	3.000	3.000
IAA production coefficient in the peripheral zone	$\rho_{IAA}(peripheral)$	5	5.000	6.000	7.500	6.000
Coefficient of additional IAA production in primordia	$\rho_{IAA}(primordium)$	6	1.000	0.000	0.000	3.500
Coefficient controlling saturation of IAA production	κ_{IAA}	5, 6	1.000	1.000	1.000	1.000
IAA decay coefficient	μ_{IAA}	5	0.100	0.100	0.100	0.100
IAA diffusion coefficient per unit cell wall length	D		4.000	4.000	4.000	4.000
IAA transport coefficient	T	3	40.000	22.500	22.000	22.500
Coefficient controlling IAA transport saturation	κT	3	1.000	1.000	1.000	1.000
IAA threshold for primordium differentiation	Th		7.500	8.000	7.000	7.500
Maximum IAA concentration	$[IAA]_{max}$	7	20.000	20.000	20.000	15.000
Base production of PIN	ρPIN_0	1	0.500	0.500	0.600	0.500
Coefficient of PIN production depending on IAA concentration	ρPIN	1	0.025	0.025	0.010	0.025
Coefficient controlling saturation of PIN production	κPIN	1	1.000	1.000	1.000	1.000
PIN decay coefficient	μPIN	1	0.100	0.350	0.350	0.350
Exponentiation base for calculating PIN relocation	b	2	3.000	3.000	3.000	3.000
Top border of peripheral zone*			2.500	2.800	4.100	2.900
Bottom border of peripheral zone†			5.000	8.400	12.300	8.700

Parameters without associated symbols are not further described in the article. The simulations use different functions to control the active ring position and size during startup. All parameters for rendering, surface and primordium shape, and surface growth are the same for all simulations. Distichous parameters are used for Movie 1 and Fig. 4*A*. Decussate parameters are used for Movie 2 and Fig. 4*B*. Tricussate parameters are used for Movie 3 and Fig. 4*C*. Spiral parameters are used for Movie 4, Fig. 4 *D*, *H*, and *I* (see also Fig. 5), and Table 2. Spiral parameters with PIN

production and decay set to 0 are used for Fig. 4 *E* and *F*.
*Steady-state distance between the apex tip and the top of the peripheral zone, measured along the generating curve.
†Steady-state distance between the apex tip and the bottom of the peripheral zone, measured along the generating curve.

Table 2. Divergence angles and primordium differentiation times for spiral phyllotaxis simulation

Primordium number	Divergence angle, °	Time, simulation steps × 100
1	0.000	2.78
2	162.740	3.00
3	96.272	6.81
4	155.880	7.20
5	123.397	10.48
6	143.205	11.05
7	139.269	14.03
8	128.599	14.87
9	142.127	16.96
10	124.750	18.48
11	144.179	19.79
12	131.910	21.46
13	125.384	22.91
14	141.180	24.34
15	132.346	26.35
16	131.631	27.37
17	124.991	29.53
18	137.307	30.88
19	135.372	32.73
20	124.094	34.03
21	122.975	35.64
22	144.799	37.08
23	114.642	38.72
24	128.862	40.15
25	133.097	42.00

26	134.966	43.74
27	142.972	45.61
28	150.016	47.05
29	130.865	49.26
30	123.537	50.10
31	132.814	52.04
32	126.695	53.46
33	136.362	55.01
34	130.081	57.07
35	134.563	58.35
36	130.904	60.03
37	135.225	61.30
38	125.441	63.02
39	153.168	64.63
40	126.086	66.63

Table 3. Divergence angles in degrees for sensitivity analysis simulations

	Primordium number									
Simulation	11	12	13	14	15	16	17	18	19	20
SA1	145.093	143.843	139.470	133.792	143.319	134.723	130.035	125.708	137.444	144.262
SA2	137.329	128.618	138.899	122.192	143.398	139.259	122.611	143.455	126.868	135.962
SA3	127.730	145.353	125.170	136.259	130.892	126.798	135.469	124.181	148.881	122.814
SA4	144.026	131.154	134.904	119.808	145.070	137.162	124.992	126.194	128.128	133.705

1. Benková, E., Michniewicz, M., Sauer, M., Teichmann, T., Seifertova, D., Jurgens, G. & Friml, J. (2003) *Cell* **115,** 591–602.

2. Ulmasov, T., Murfett, J., Hagen, G. & Guilfoyle, T. J. (1997) *Plant Cell* **9,** 1963–1971.

3. Smith, C., Prusinkiewicz, P. & Samavati, F. (2003) *Lecture Notes in Computer Science* (Springer, Berlin) Vol. 3062, pp. 313–327.

4. Kramer, E. M. (2002) *J. Theor. Biol.* **216,** 147–158.

5. Nakielski, J. (2000) in *Pattern Formation in Biology*, *Vision*, *and Dynamics*, eds. Carbone, A., Gromov, M. & Prusinkiewicz, P. (World Scientific, Singapore), pp. 252–267.

6. Hejnowicz, Z., Nakielski, J. & Hejnowicz, K. (1984) *Acta Soc. Bot. Pol.* **53,** 301–316.

7. Mündermann, L., Erasmus, Y., Lane, B., Coen, E. & Prusinkiewicz, P. (2005) *Plant Physiol.* **139,** 960–968.

8. Silk, W. K. & Erickson, R. O. (1979) *J. Theor. Biol.* **76,** 481–501.

9. Richards, O. W. & Kavanagh, A. J. (1943) *Amer. Nat.* **77,** 385–399.

10. Kwiatkowska, D. & Dumais, J. (2003) *J. Exp. Bot.* **54,** 1585–1595.

11. Reddy, G. V., Heisler, M. G., Ehrhardt, D. W. & Meyerowitz, E. M. (2004) *Development (Cambridge, U.K.)* **131,** 4225–4237.